Measuring spectral distortion anisotropies with the Square Kilometer Array

David Zegeye, Thomas Crawford, Jens Chluba, Matthieu Remazeilles, and Keith Grainge

Based on: 2406.04326
2303.00916

CMB power spectrum and Gaussianity

Disconnected regions of Cosmic Microwave Background (CMB) temperature anisotropies are correlated and nearly scale-invariant

Perturbations believed to be quantum-scale fluctuations stretched to macroscopic scales by inflation

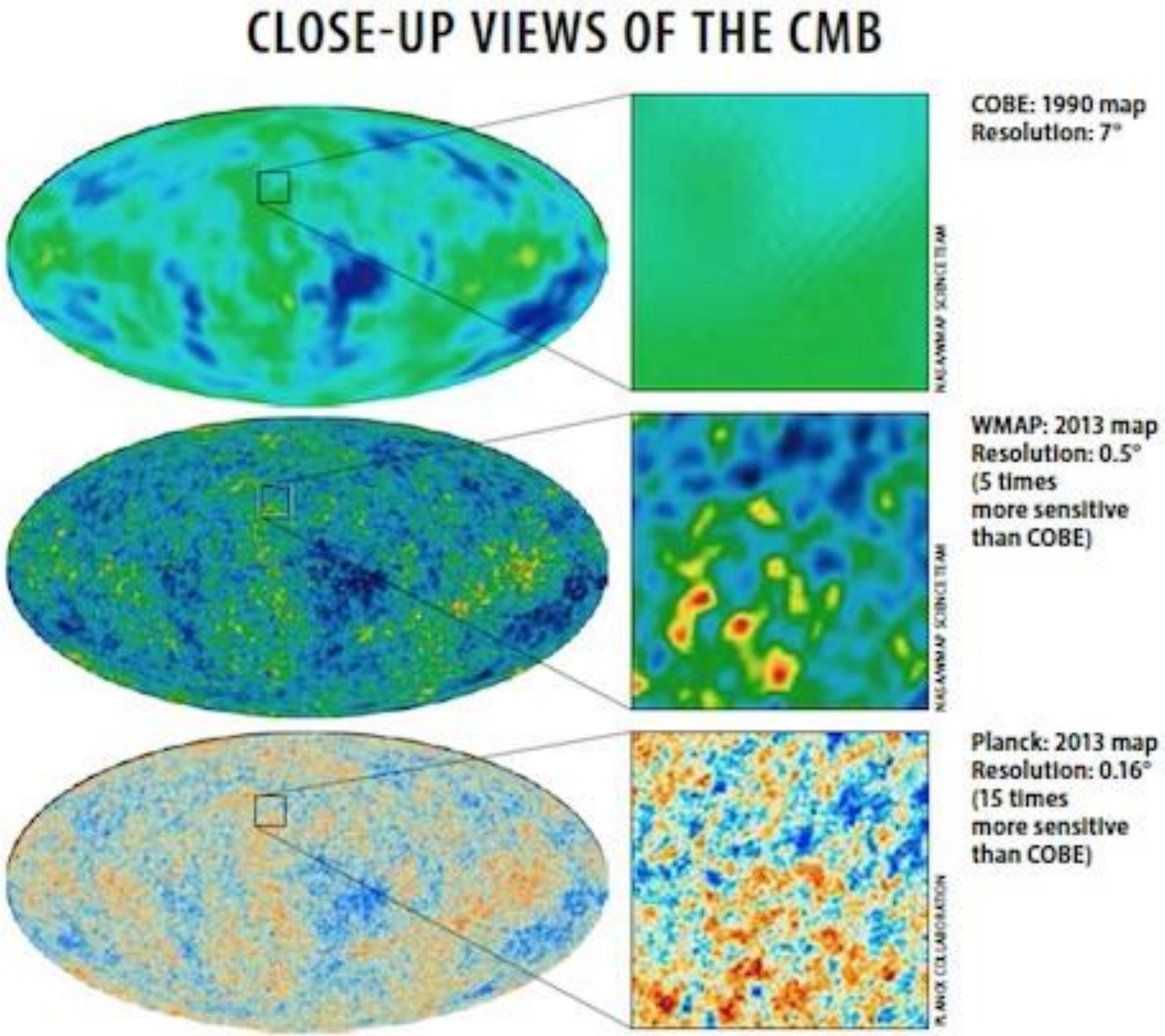

CMB power spectrum and Gaussianity

For non-interacting quantum fields, perturbations follow a Gaussian distribution. Can parameterize non-Gaussianity as:

$$\Phi = \Phi_G + f_{NL}\Phi_G^2$$

Planck 2018 constrains the primordial power spectrum around $k_* \approx 0.05\ Mpc^{-1}$, as well as $f_{NL} < 10$. Upcoming surveys will reach $f_{NL} \sim O(1)$.

Planck (2018)

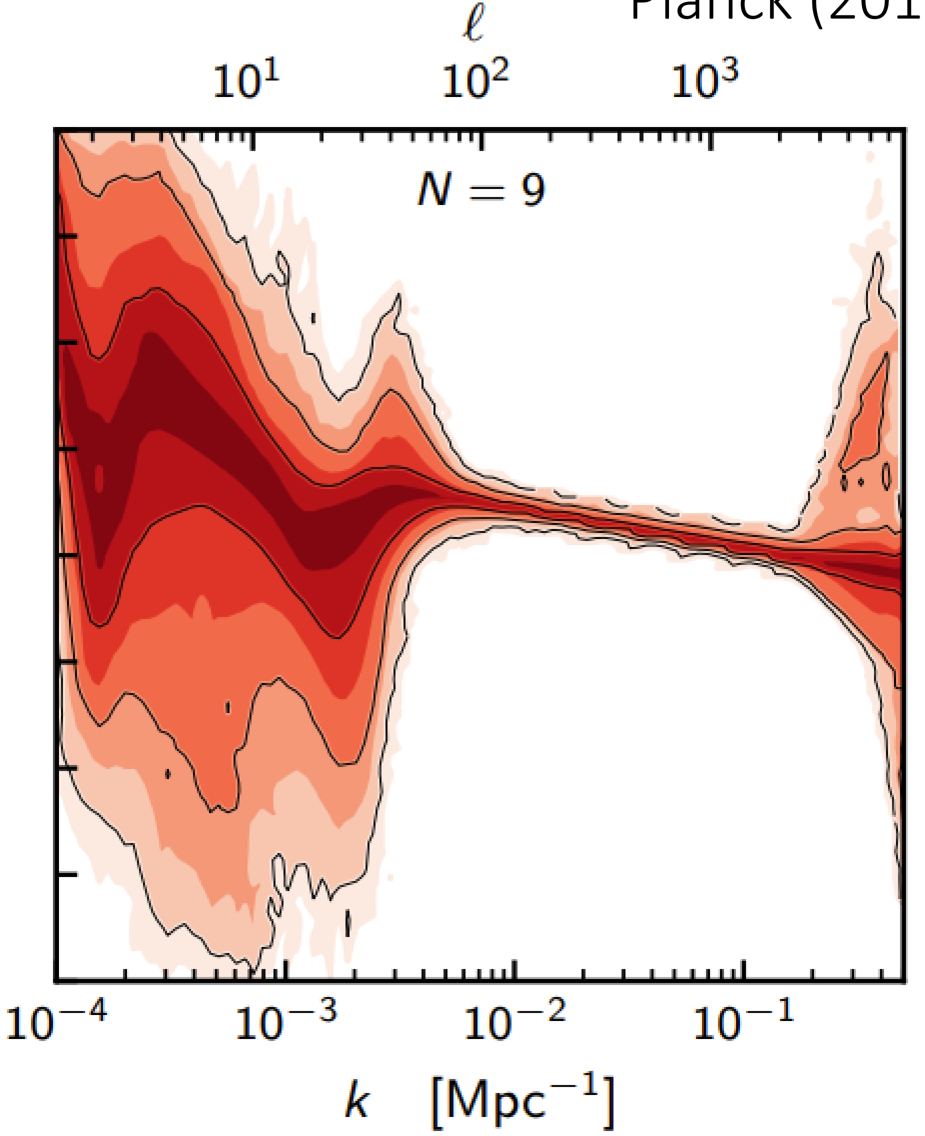

Probing small-scales: μ-Distortions

For $5 \times 10^4 < z < 2 \times 10^6$, energy injections thermalized through distorting the CMB blackbody:

$$\frac{1}{e^x - 1} \to \frac{1}{e^{x+\mu} - 1}$$

$$\mu \approx 1.4 \frac{\delta E}{E}$$

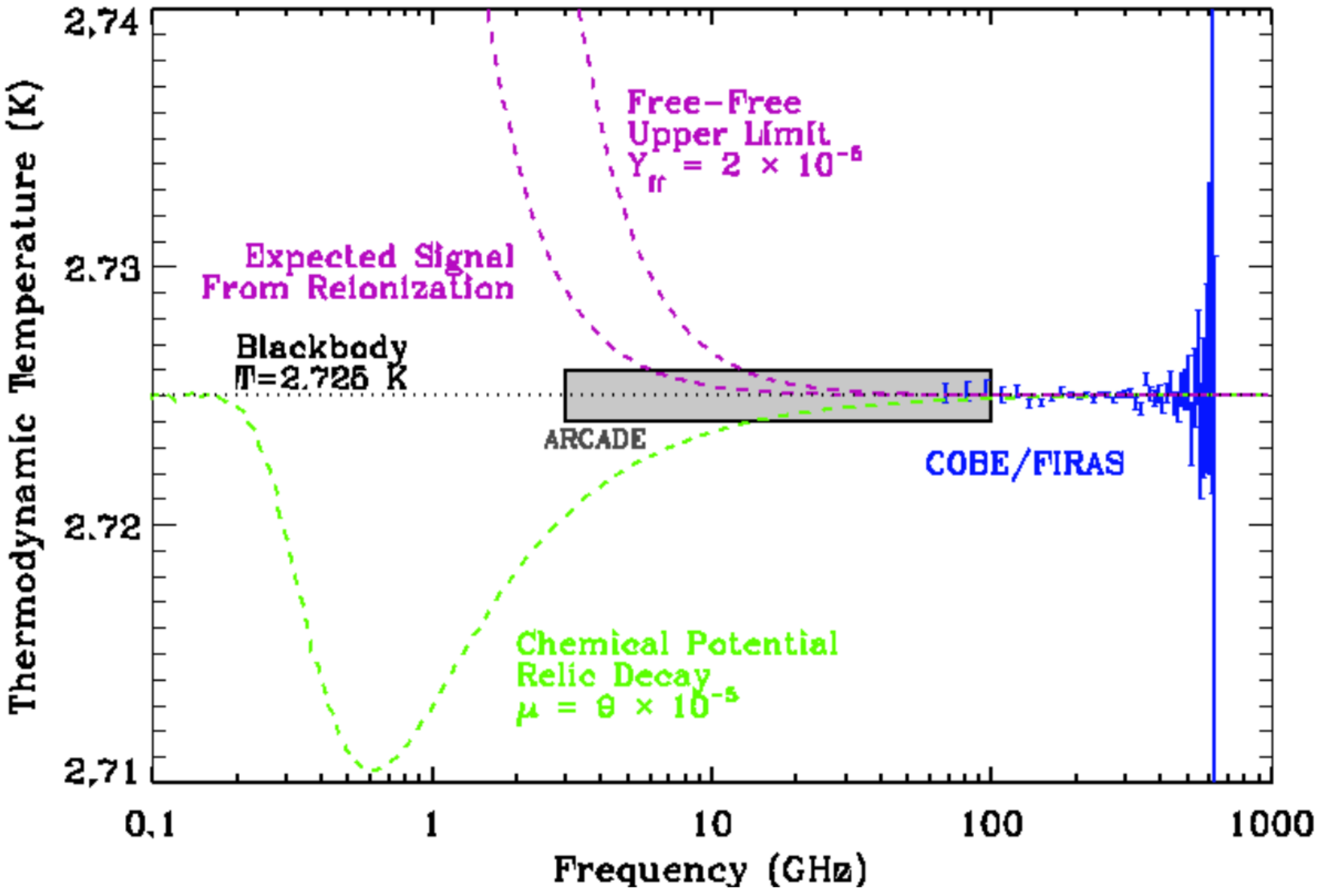

ARCADE

Small-scale power spectrum

Since photons are redistributing energy across the plasma, acts as a form of energy injection into the bath

$$\frac{\delta E}{E} \propto \int \frac{\mathrm{dk}}{2\pi} k^2 P(k) W(k)$$

μ traces small-scale power!

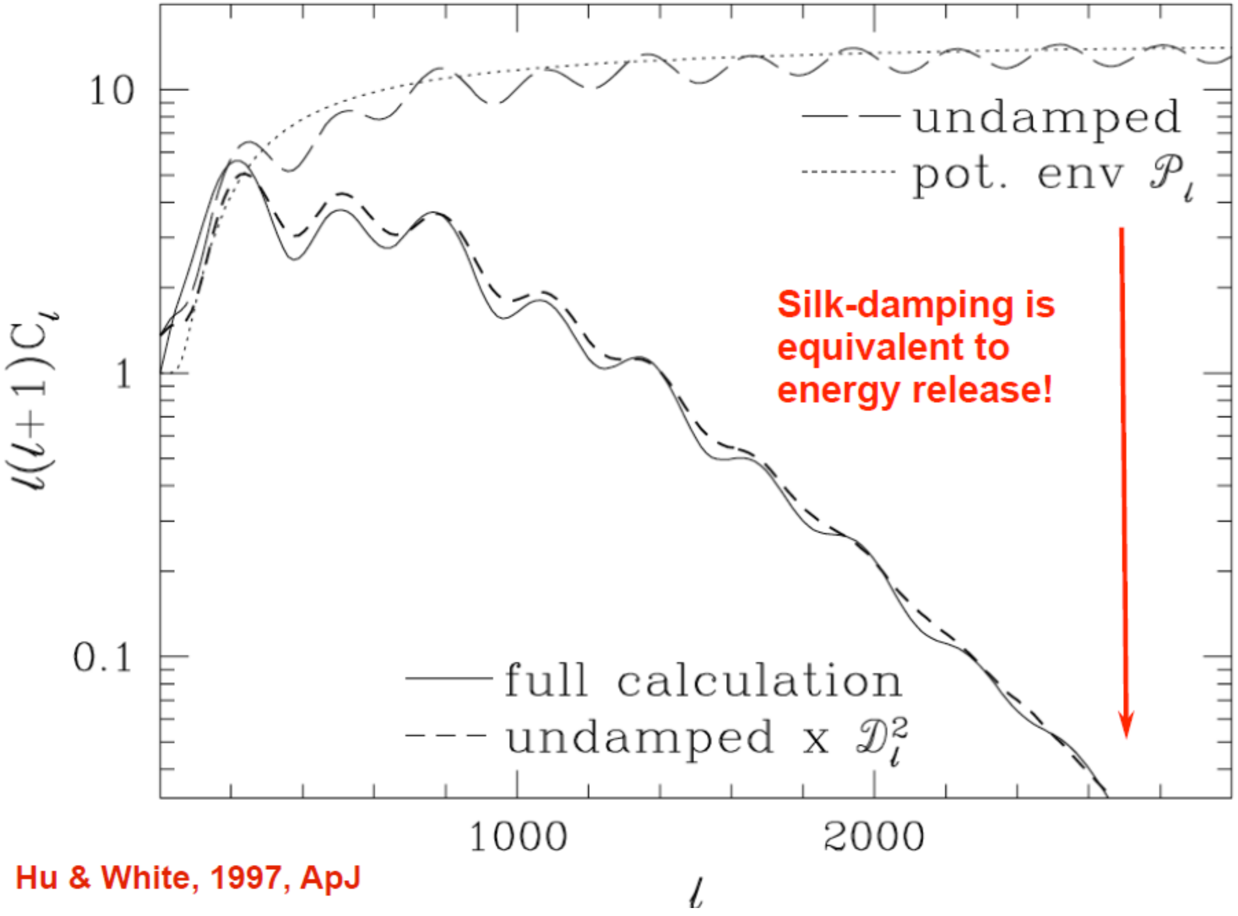

Hu & White, 1997, ApJ

μ-anisotropies from perturbation theory

Perturbations in the metric and heating rate induce μ-anisotropies from an initially isotropic μ-distortion

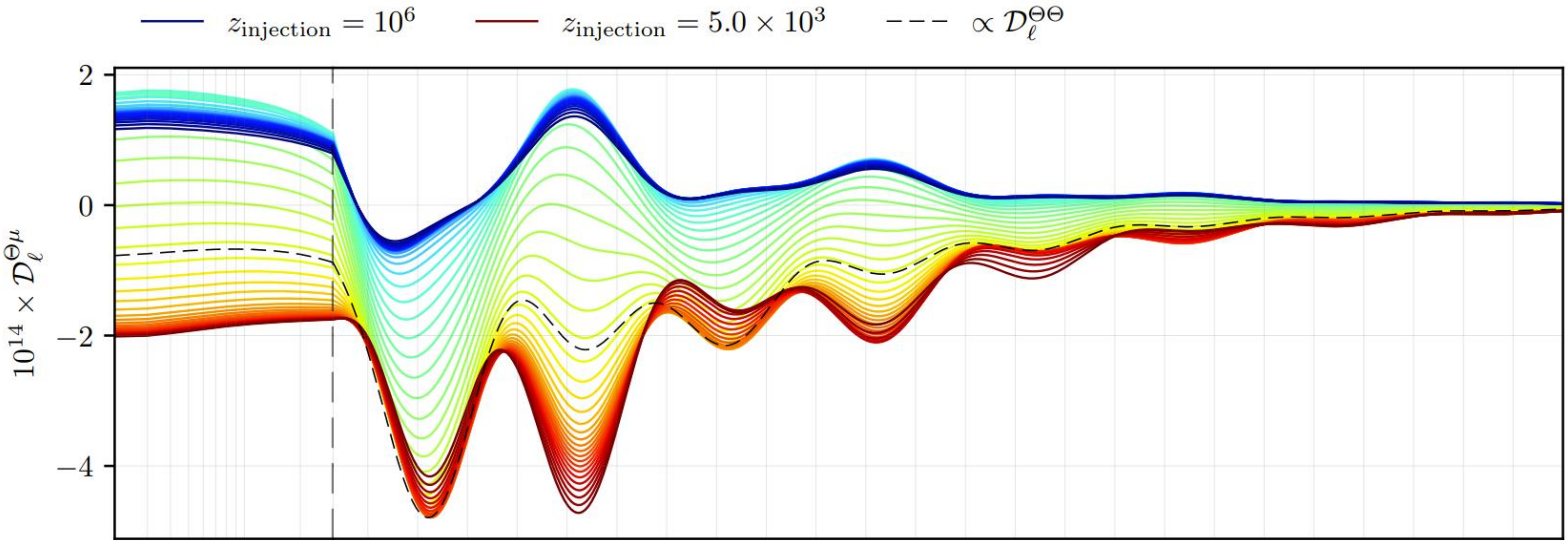

Kite et al (2022)

μ-anisotropies from non-Gaussianity

Anisotropies in μ exist if long-wavelength modes of size k_L modulate the amplitude of small-scale power [i.e. spatially-varying $P_\zeta(k_s)$]

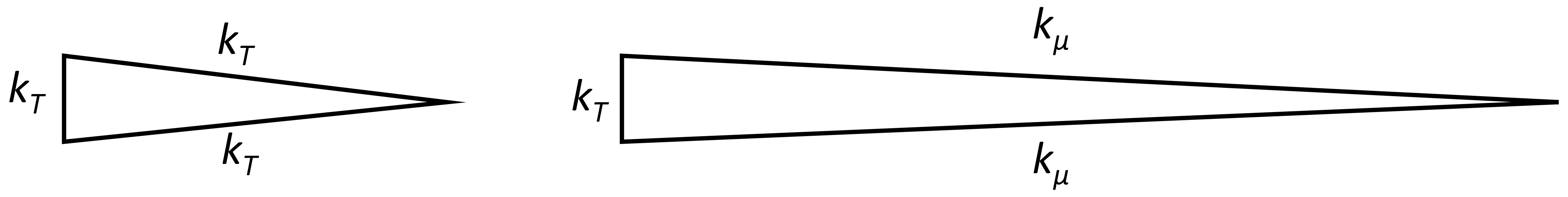

$\langle TTT \rangle$ $\langle \mu T \rangle$

μ-distortions are useful for probing non-gaussianity at small scales $\left(k_\mu \approx 10^4\ Mpc^{-1}\right)$

Constraining small-scale power & non-Gaussianity

$$\delta\mu_{evo} \sim \langle\mu\rangle\zeta_L$$

$$\delta\mu_{f_{NL}} \sim f_{NL}\langle\mu\rangle\zeta_L$$

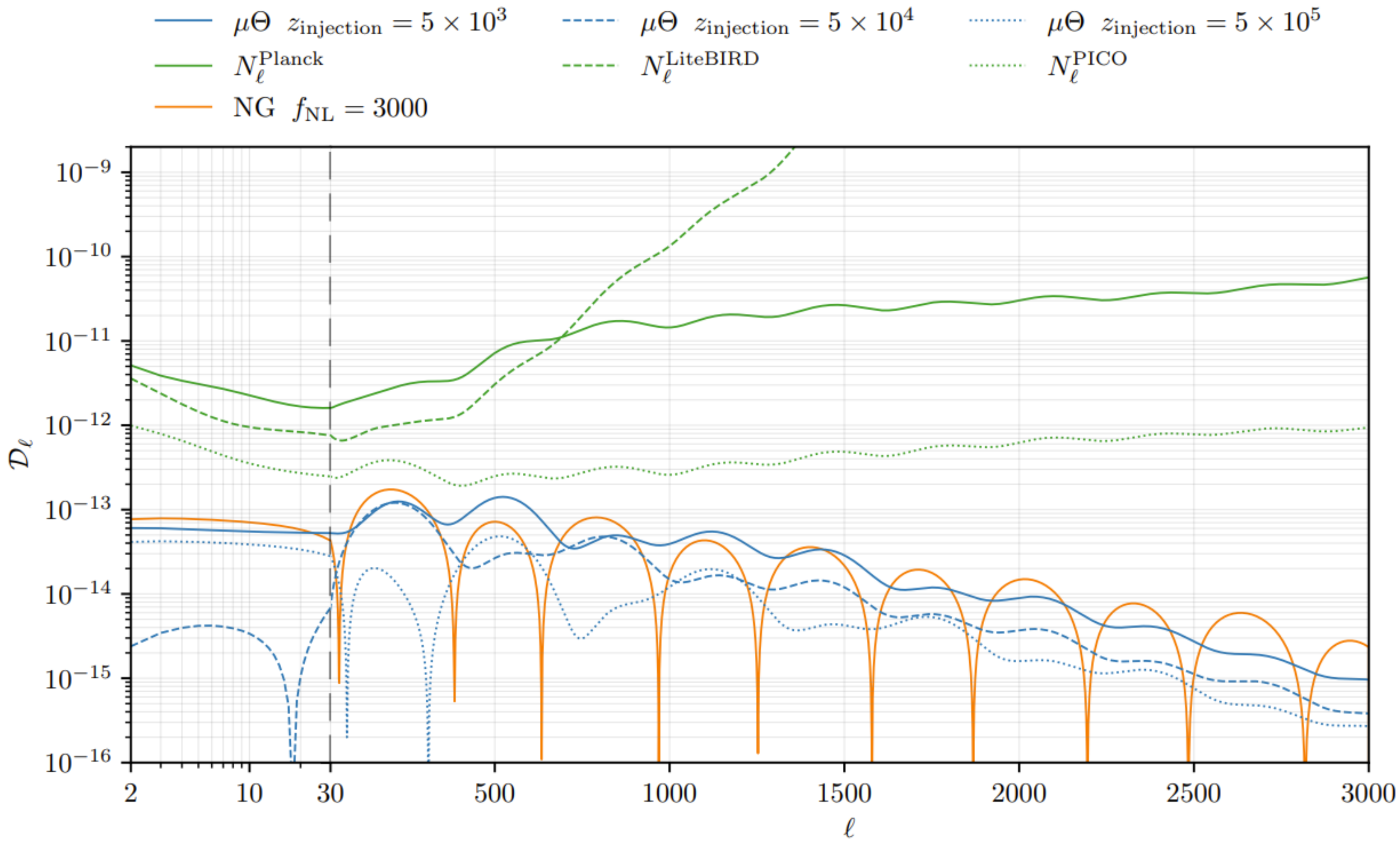

Kite et al (2022)

Foregrounds strongly obscure μ-distortions

Remazeilles & Chluba (2018)

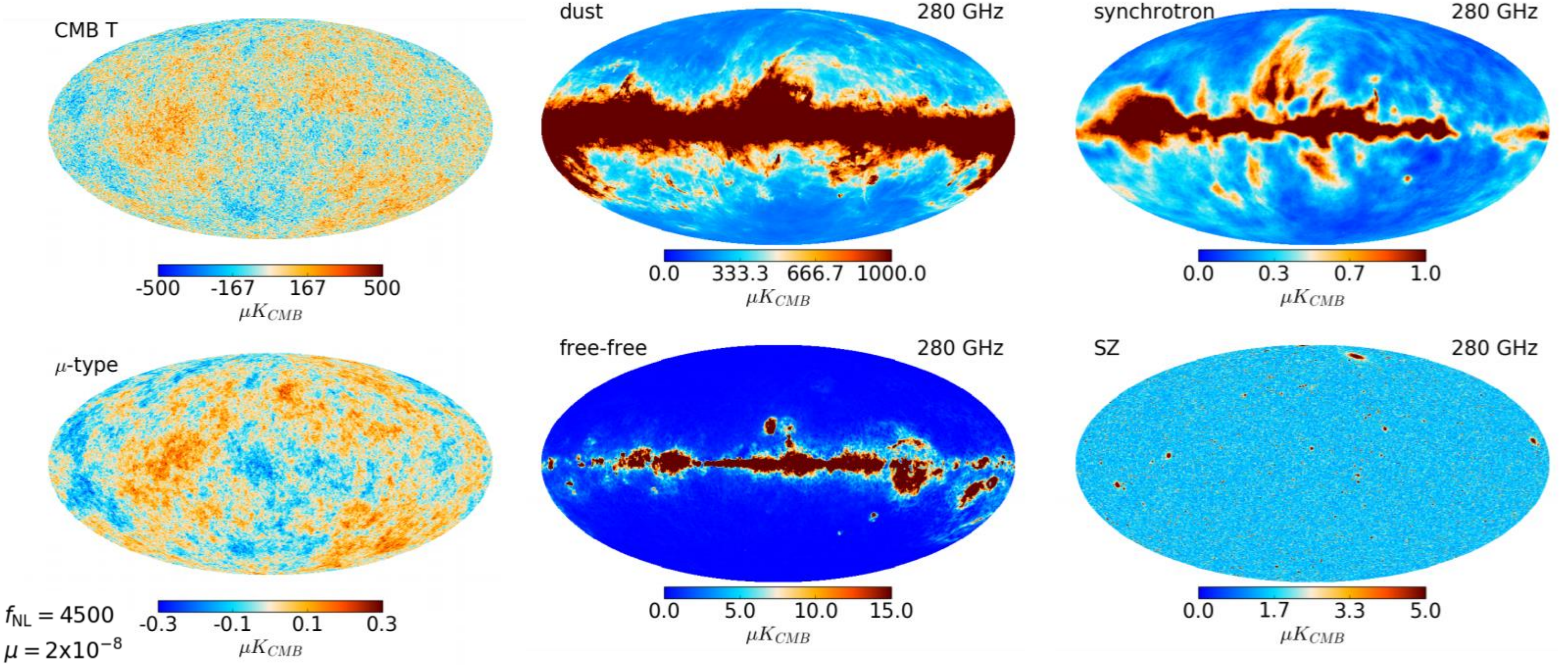

For CMB-S4, atmosphere weakens our low-ℓ signal

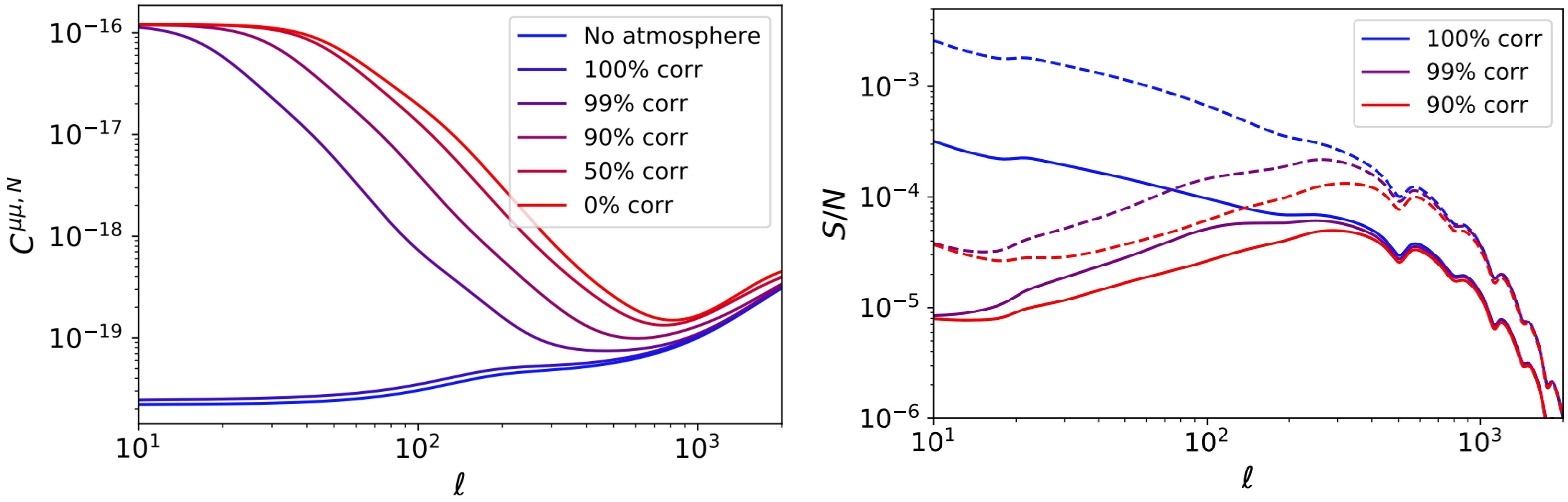

Zegeye et al (2023a)

Survey ($\mu = 2 \times 10^{-8}$)	$\sigma(f_{NL})$	$\sim \sigma(\mu)$
CMB-S4 (Deep; 99% atmo. corr.)	804 (246)	$\sim 2 \times 10^{-5}$ ($\sim 5 \times 10^{-6}$)
LiteBIRD (Remazeilles et al 2021)	826 (91)	$\sim 2 \times 10^{-5}$ ($\sim 2 \times 10^{-6}$)

Improving constraints for ground-based survey

- More frequency channels to clean out foregrounds
- Since atmosphere is the main challenge, want to observe at frequencies where atmosphere is reduced and detectors where atmosphere is highly correlated
- Most noticeable, μ signal peaks at low frequencies

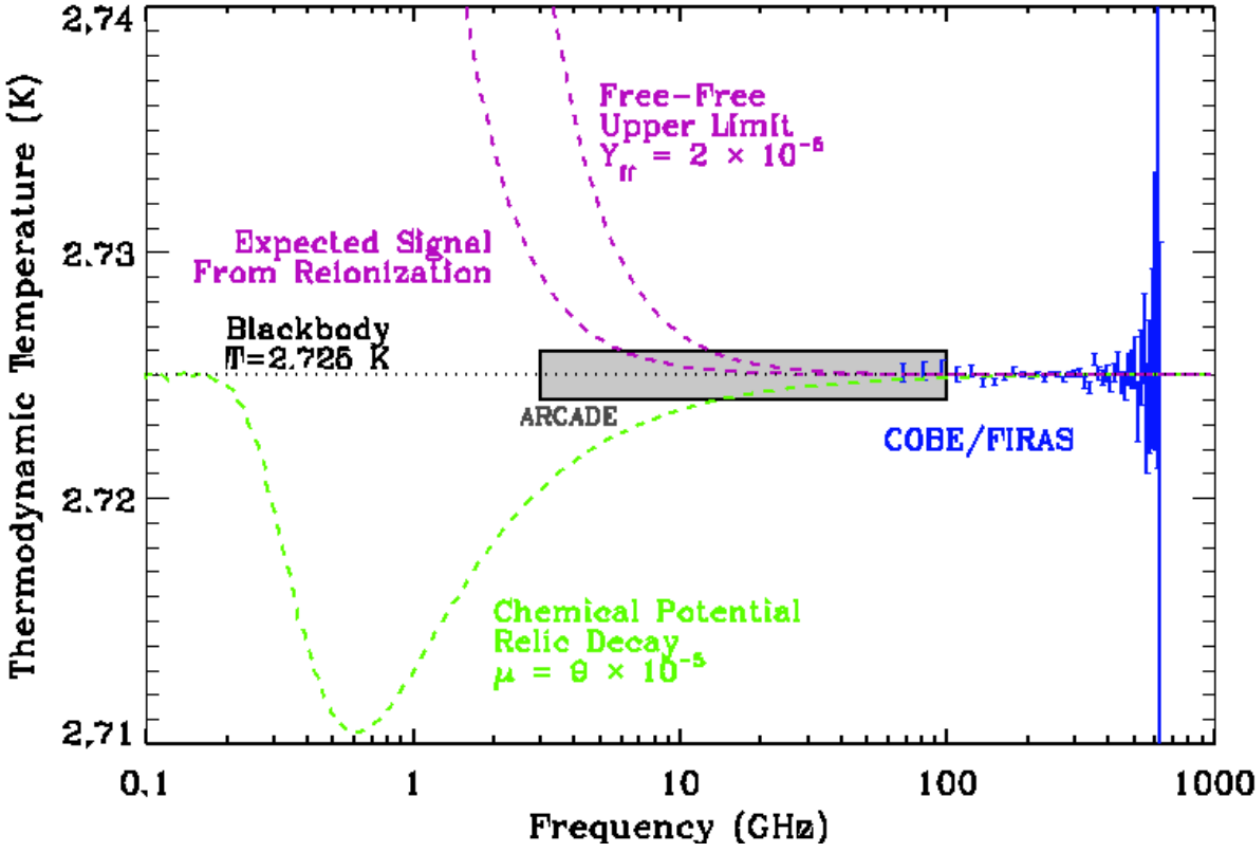

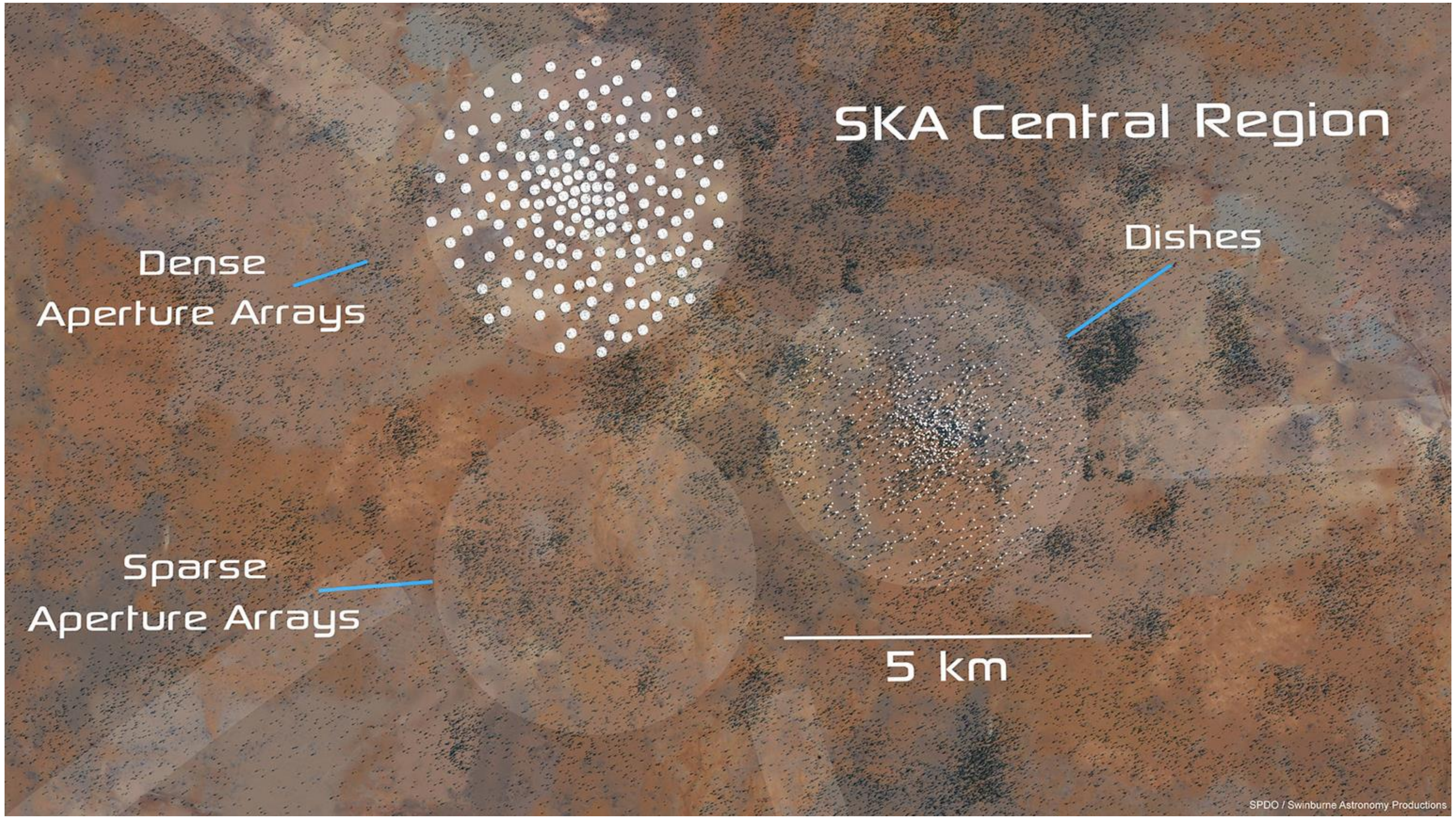

The Square Kilometer Array is expected to observe from 350 MHz - 15 GHz, with access to 1000s of frequency channels

Noise level comparison

Survey	Survey area	N_{dish}
SKA1-Mid	20,000 deg^2	133+64 (MeerKat)

- SKA radio dish can operate in "single-dish" mode

- SKA1 with a single channel, $\Delta\nu = 1\ GHz, t = 1\ yr$:

$$\sqrt{C^{TT}} \sim 20\ \mu k - arcmin,$$
$$\sqrt{C^{\mu\mu}} \sim 4\ \mu k - arcmin$$

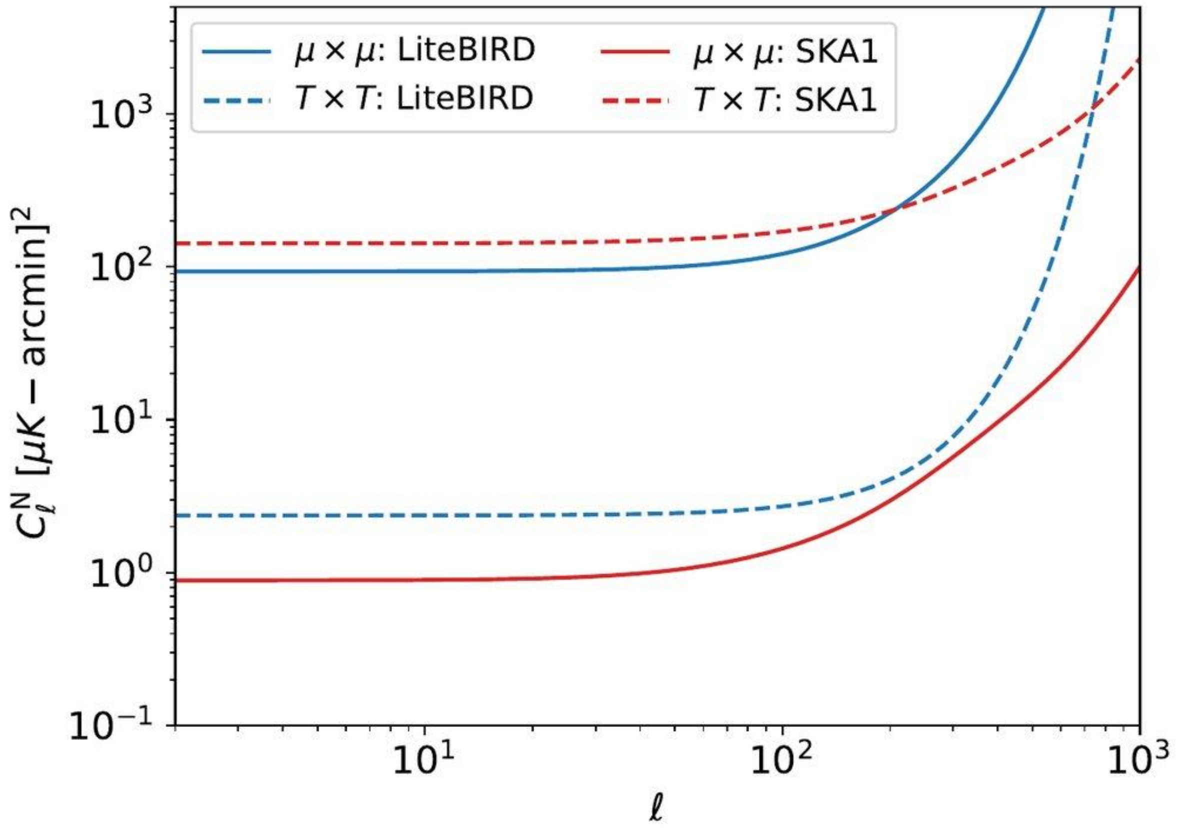

“Red”-Noise

Atmosphere appears to be negligible in MeerKAT data, but time-correlated noise ($1/f$) will lead to large-scale features in our maps. The point at which the frequency associated with red-noise is comparable to the white-noise levels is the “knee”-frequency, f_k.

From MeerKAT data, $f_k \sim \mathbf{0.1}\ Hz$, impacting $\ell < \mathbf{50}$. Li et al (2020) find red-noise is >99% correlated between frequency bands (0.96 - 1.67 GHz) and can be subtracted to levels below instrumental noise.

Complex foregrounds

Assumption for S4-only forecast is smooth foregrounds

Spatial variation of spectral index complicates our ability to describe foregrounds with a single SED

Synchrotron will easily be the most significant foreground impacting μ at low frequencies

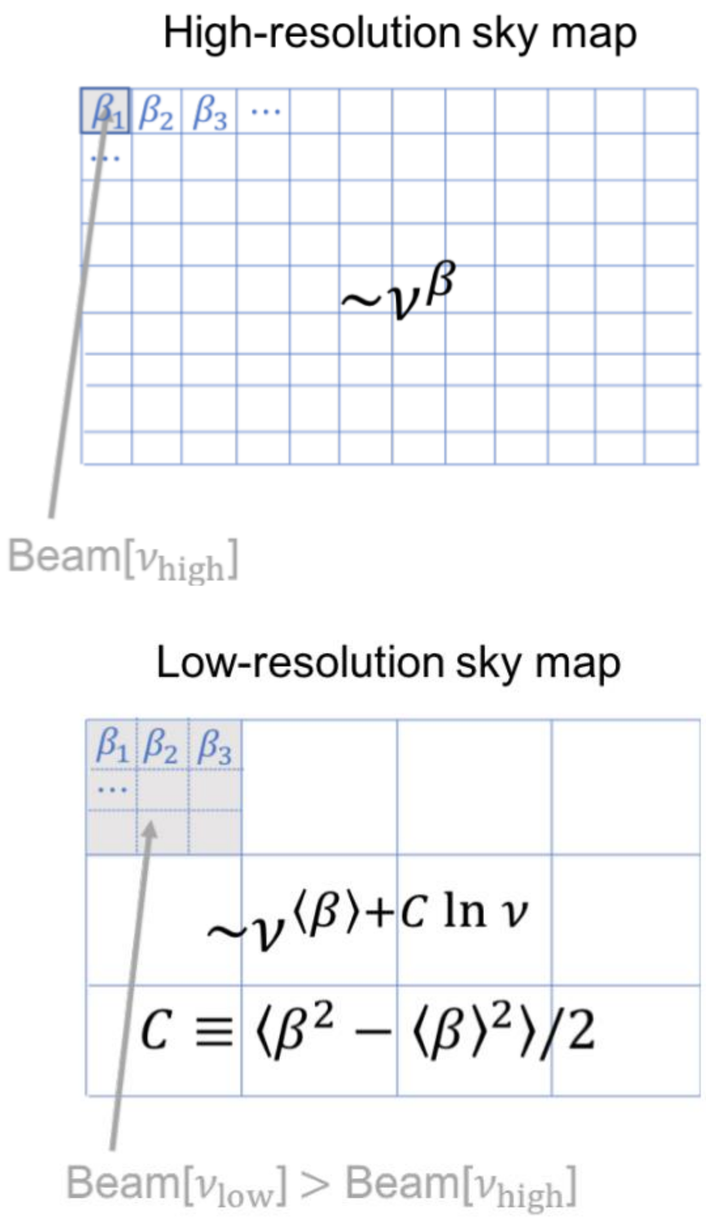

Complex foregrounds

Perform a perturbative expansion around β to account for spatial variation

$$f(\nu,\bar{\beta},\beta) = f_0(\nu,\bar{\beta}) + \sigma(\beta)\partial_{\bar{\beta}} f_0(\nu,\bar{\beta}) + \sigma(\beta)^2 \partial_{\bar{\beta}}\partial_{\bar{\beta}} f_0(\nu,\bar{\beta}) + \cdots$$

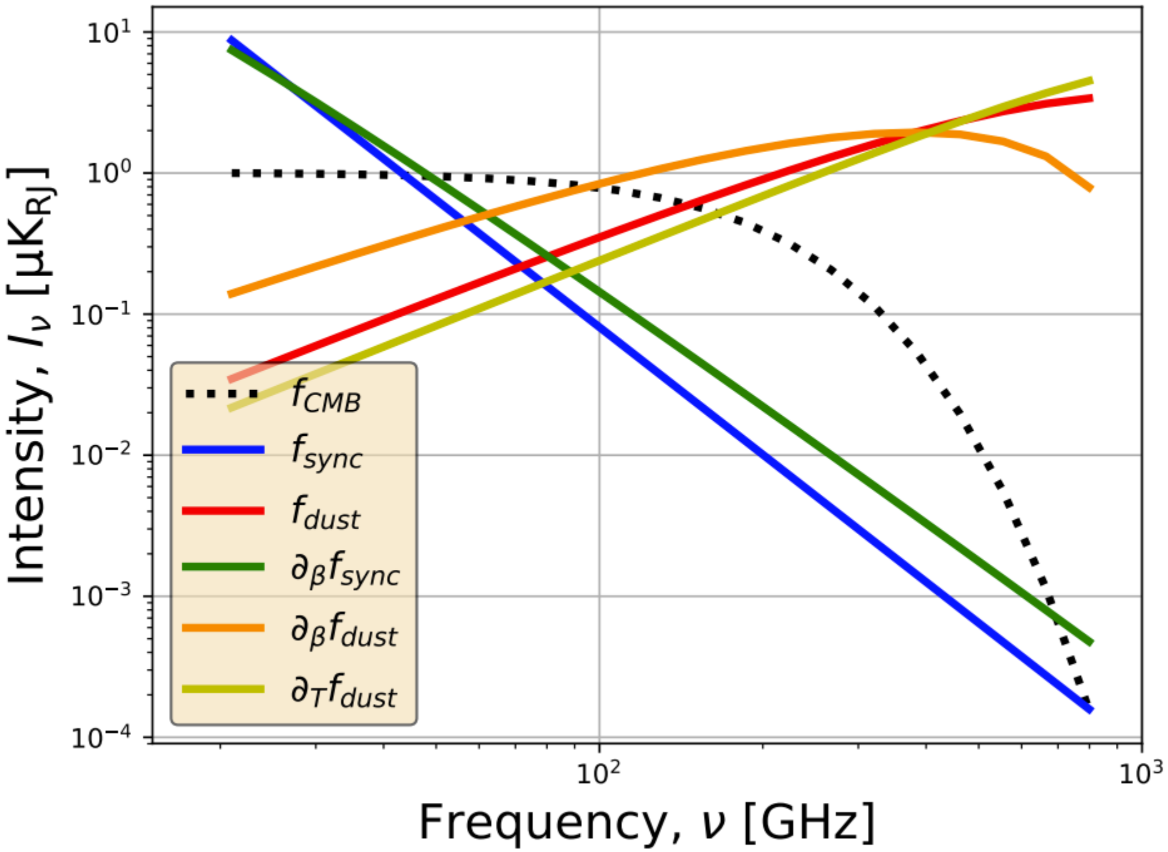

This analytic approach likely more pessimistic than if we did a map-based analysis

Survey ($\mu = 2 \times 10^{-8}$)	$\sigma(f_{NL})$	$\sim \sigma(\mu)$
SKA1 only	$31 - 234$ (8)	$6 \times 10^{-7} - 5 \times 10^{-6}$ (2×10^{-7})
SKA1+LiteBIRD	$23 - 92$ (6)	$5 \times 10^{-7} - 2 \times 10^{-6}$ (1×10^{-7})

Parameter space (for illustration purposes!)

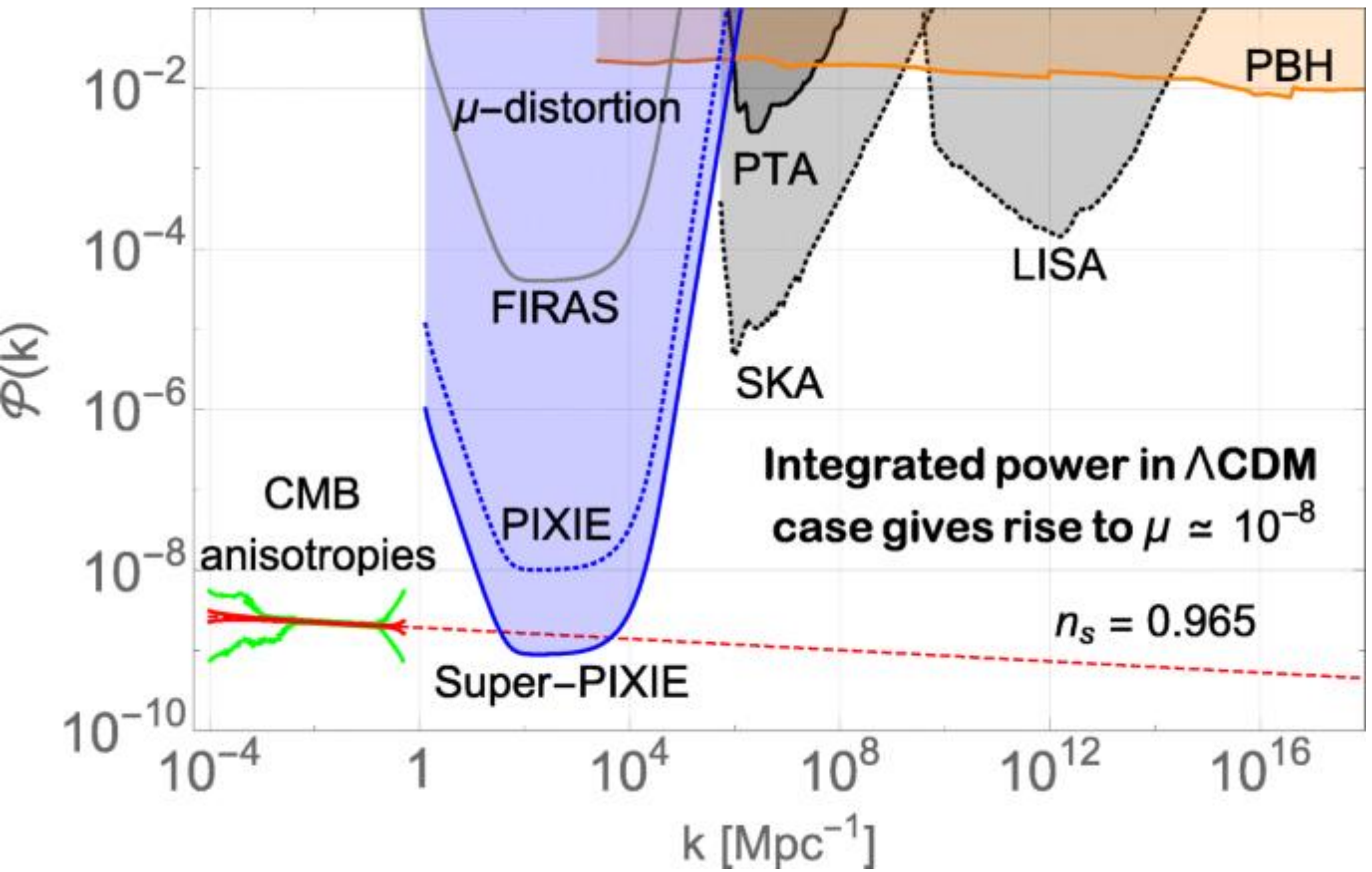

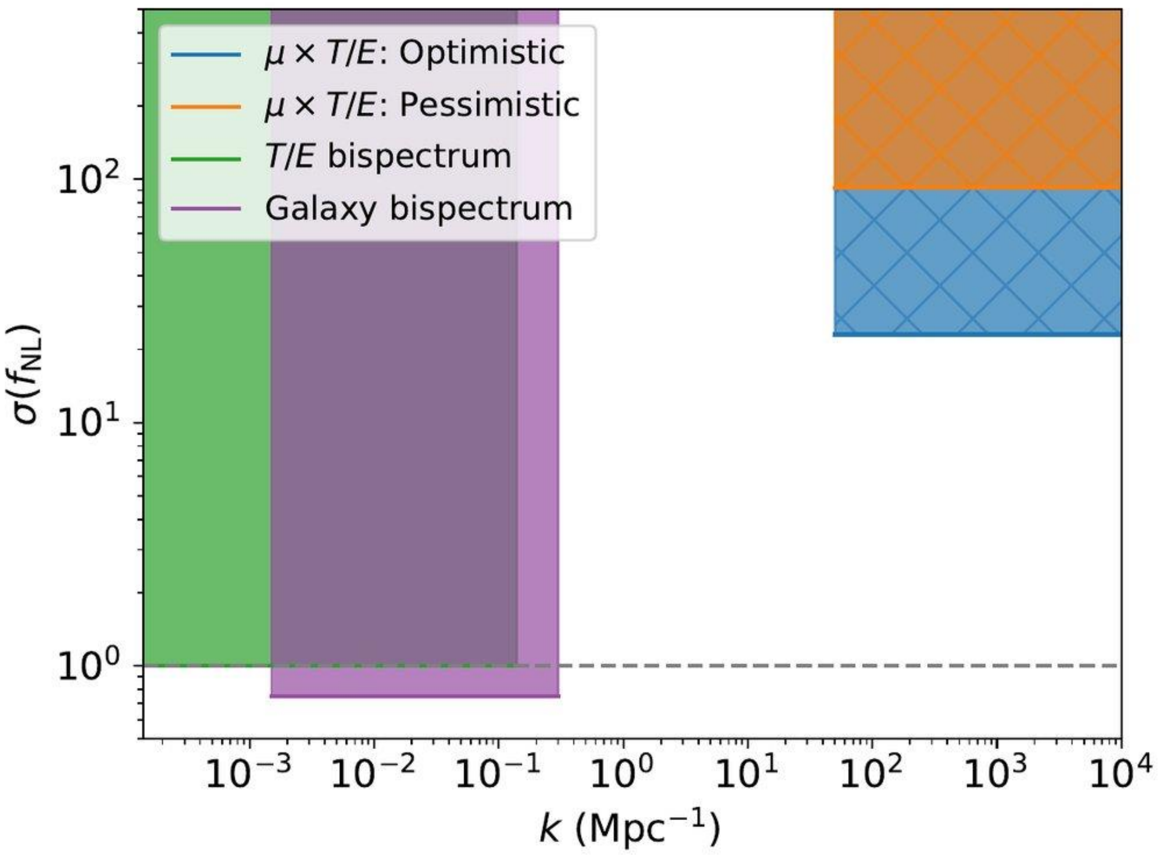

Chluba et al (2019)

Conclusion & future steps

SKA in single-dish mode can improve constraints on the power spectrum and f_{NL} from μ-anisotropies. Need simulations-based forecast to fully understand effects of spatially-varying foreground parameters!

Since atmosphere and foreground removal is better, potential for use in measuring B-modes.

Interferometer mode could improve measurements of the primary CMB and secondaries at $\ell > 5000$, potential for joint analysis with high-resolution CMB experiments like S4 or HD.

Extra Slides

Boltzmann Equation

$$\frac{\partial \boldsymbol{y}_0^{(0)}}{\partial \eta} = \tau' \theta_z \left[M_{\mathrm{K}} \boldsymbol{y}_0^{(0)} + \boldsymbol{D}_0^{(0)} \right] + \frac{\boldsymbol{Q}'^{(0)}}{4}, \tag{2.1a}$$

$$\frac{\partial \boldsymbol{y}^{(1)}}{\partial \eta} + \hat{\boldsymbol{\gamma}} \cdot \nabla \boldsymbol{y}^{(1)} = -\boldsymbol{b}_0^{(0)} \left(\frac{\partial \Phi^{(1)}}{\partial \eta} + \hat{\boldsymbol{\gamma}} \cdot \nabla \Psi^{(1)} \right) + \tau' \left[\boldsymbol{y}_0^{(1)} + \frac{1}{10} \boldsymbol{y}_2^{(1)} - \boldsymbol{y}^{(1)} + \beta^{(1)} \chi \, \boldsymbol{b}_0^{(0)} \right] + \frac{\boldsymbol{Q}'^{(1)}}{4} \tag{2.1b}$$

$$+ \tau' \theta_z \left\{ M_{\mathrm{K}} \boldsymbol{y}_0^{(1)} + \boldsymbol{D}_0^{(1)} + \left[\delta_{\mathrm{b}}^{(1)} + \Psi^{(1)} \right] \left(M_{\mathrm{K}} \boldsymbol{y}_0^{(0)} + \boldsymbol{D}_0^{(0)} \right) + \Theta_0^{(1)} \left(\boldsymbol{D}_0^{(0)} + M_{\mathrm{D}} \boldsymbol{y}^{(0)} - \boldsymbol{S}^{(0)} \right) \right\},$$

$$\boldsymbol{D}^{(0)} = \left(\gamma_T x_{\mathrm{c}} \mu^{(0)}, 0, 0, \ldots, 0, -\gamma_N x_{\mathrm{c}} \mu^{(0)} \right)^T, \qquad \boldsymbol{D}^{(1)} = \left(\gamma_T x_{\mathrm{c}} \mu^{(1)}, 0, 0, \ldots, 0, -\gamma_N x_{\mathrm{c}} \mu^{(1)} \right)^T,$$

$$\dot{\boldsymbol{Q}}^{(0)} = \left(0, \frac{\dot{Q}_{\mathrm{c}}^{(0)}}{\rho_z}, 0, \ldots, 0, 0 \right)^T, \qquad \dot{\boldsymbol{Q}}^{(1)} = \left(0, \frac{\dot{Q}_{\mathrm{c}}^{(1)}}{\rho_z} + \Psi^{(1)} \frac{\dot{Q}_{\mathrm{c}}^{(0)}}{\rho_z}, 0, \ldots, 0, 0 \right)^T,$$

$$\boldsymbol{S}^{(0)} = \left(0, \delta_{\gamma,0}^{(0)} + 4\Theta_{\mathrm{e}}^{(0)}, -4\Theta_{\mathrm{e}}^{(0)}, \ldots, 0, 0 \right)^T,$$

$$\boldsymbol{y} = (\Theta, y, y_1, \ldots, y_n, \mu)^{\mathrm{T}}$$

μ-anisotropies from isotropic y-distortions